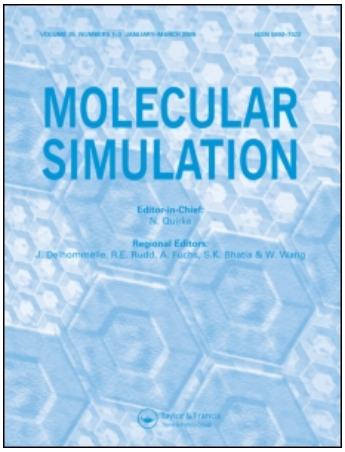

Molecular Simulation
Publication details, including instructions for authors and subscription information:
http://www.informaworld.com/smpp/title~content=t713644482

Comparison of rheological properties of short-chain perfluoropolyethers through simulation and experiment

B. Jiang[a]; N. J. Crawford[b]; D. J. Keffer[a]; B. J. Edwards[a]; J. L. Adcock[b]
[a] Department of Chemical Engineering, The University of Tennessee, Knoxville, TN, USA [b] Department of Chemistry, The University of Tennessee, Knoxville, TN, USA

To cite this Article Jiang, B. , Crawford, N. J. , Keffer, D. J. , Edwards, B. J. and Adcock, J. L.(2007) 'Comparison of rheological properties of short-chain perfluoropolyethers through simulation and experiment', Molecular Simulation, 33: 9, 871 — 878
To link to this Article: DOI: 10.1080/08927020701275035
URL: http://dx.doi.org/10.1080/08927020701275035

Molecular Simulation, Vol. 33, Nos. 9–10, 15–30 August 2007, 871–878

Taylor & Francis
Taylor & Francis Group

Comparison of rheological properties of short-chain perfluoropolyethers through simulation and experiment

B. JIANG†, N. J. CRAWFORD‡, D. J. KEFFER†*, B. J. EDWARDS† and J. L. ADCOCK‡

†Department of Chemical Engineering, The University of Tennessee, Knoxville, TN 37996-2200, USA
‡Department of Chemistry, The University of Tennessee, Knoxville, TN 37996-2200, USA

(Received October 2006; in final form February 2007)

Four short-chain perfluoropolyethers (PFPEs) with varied architectural modifications have been studied rheologically using non-equilibrium molecular dynamics simulation and experiment. An explicit-atom potential, which treats all fluorine atoms equivalently, is not capable of reproducing the experimentally observed trends in viscosity among the four compounds. Rather, the parameters of the potential governing the interaction of fluorine must reflect the proximity of the fluorine to the oxygen in the ether linkage. Defining four different types of fluorine atoms, we are able to reproduce the experimentally observed trends in viscosity among the four compounds. We examine the effect of this potential change on the structural properties as well.

Keywords: Perfluoropolyethers; PFPE; Lubrication; Viscosity; Nonequilibrium molecular dynamics; Interaction potential

1. Introduction

Perfluoropolyethers (PFPEs) have been used as lubricants for decades due to their chemical inertness, thermal stability, non-flammability, radiation stability and low vapor pressures, in a diverse range of industries from aerospace applications to magnetic recording media [1,2]. In particular, the steady increase in recording density leads to very severe conditions for the head/disk interface, such as extremely high shear rates on the disk. The rheological properties are crucial to the performance of the lubricant in these cases [3].

The PFPE fluids and greases have been extensively studied experimentally [1]. Evaluation of different types of commercially available PFPEs were carried out by Snyder *et al.* [2,4,5] through the reciprocating and four-ball tribometers, simulating dynamic bearing conditions. Most of this research targeted military applications, such as gas-turbine engine oil. This research revealed useful insights on the structure/property relationships at the macroscopic level, such as the destabilizing effect of an $-OCF_2O-$ group. Other research groups [1,6,7] studied the rheological properties of PFPE fluids as well. Jhon *et al.* [7–10] focused on the application of PFPEs in recording media both experimentally and via non-equilibrium molecular dynamics (NEMD) using a coarse–grained bead-spring model. Li *et. al* [11] also used a coarse-grained bead/spring model to investigate a nanoscale film interacting with different walls. Two publications [12,13] presented the transport properties of PFPEs confined by two rigid walls with molecular dynamics; atomic-scale force field and friction coefficients were determined at several temperatures.

In previous work [14], we reported rheological properties and structural and energetic properties of one linear compound, $C_8F_{18}O_4$ ($CF_3O(CF_2CF_2O)_3CF_3$), both at equilibrium and under shear flow. In this contribution, atomistic simulation has been applied to four short-chain PFPEs. Both equilibrium and non-equilibrium molecular simulations are applied to the previously studied compound and three other linear PFPEs: $C_6F_{14}O_3$ ($CF_3O(CF_2CF_2O)_2CF_3$), $C_8F_{18}O_3$ ($CF_3CF_2O(CF_2CF_2O)_2CF_2CF_3$) and $C_7F_{16}O_4$ ($CF_3OCF_2CF_2OCF_2OCF_2CF_2OCF_3$). The structures are depicted in figure 1. We examine herein the effect of how the fluorines are described through the interaction potential on both the rheological and structural properties.

We chose the four PFPEs in figure 1 on the following basis. The top compound, $C_8F_{18}O_4$ (*base*), is our base case model. Each of the three internal repeat units is composed

*Corresponding author. Email: dkeffer@utk.edu

Molecular Simulation
ISSN 0892-7022 print/ISSN 1029-0435 online © 2007 Taylor & Francis
http://www.tandf.co.uk/journals
DOI: 10.1080/08927020701275035

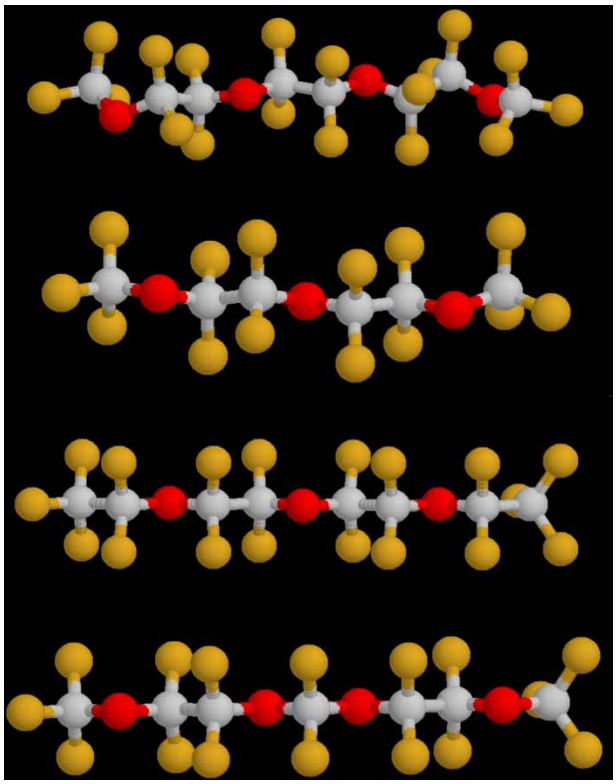

Figure 1. Schematic of PFPE lubricant structures: from top, (a) $C_8O_4F_{18}$ (*base*); (b) $C_6O_3F_{14}$ (*short*); (c) $C_8O_3F_{18}$ (*end*); and (d) $C_7O_4F_{16}$ (*OCO*). Carbon atoms are gray, oxygen are red and fluorine are gold.

of two carbon atoms capped with single carbon end groups. The second compound, $C_6F_{14}O$ (*short*), differs from the *base* compound only in that it has two internal repeat units, rather than three. By comparing the *base* PFPE and the *short* PFPE, we observe the effect of chain length. The third compound, $C_8F_{18}O_3$ (*end*), differs from the *short* compound only in that it has larger end groups, composed of two carbon atoms rather than one. By comparing the *short* PFPE and the *end* PFPE, we observe the effect of size of the end group. The fourth compound, $C_7F_{16}O_4$ (OCO), differs from the *base* compound only in that its central repeat unit has an OCO group rather than an OCCO group. By comparing the *base* PFPE and the OCO PFPE, we observe the effect of the OCO group.

The remainder of this paper is organized as follows. The interaction potential, simulation technique, and experimental details are described in the next section. Comparison of the rheological properties of the four linear PFPE compounds between simulation and experiment is presented in Section 3. Finally, the conclusions are presented in Section 4.

2. Molecular dynamics simulation and experimental methods

2.1 Interaction potentials

The base force field we used in this research is the universal force field (UFF) developed by Rappe *et al.* [15]. The UFF potential is an explicit atom potential. We chose to use an explicit atom potential since previous work had demonstrated that, while united-atom models can satisfactorily generate transport properties for hydrocarbons, they introduce significant errors for fluorocarbons due to the increased size of the fluorine atom [16]. The UFF potential includes: (i) bond stretching, (ii) bond bending, (iii) dihedral bond torsion, and (iv) intramolecular and intermolecular non-bonded interactions via a Lennard–Jones 12–6 potential. The UFF potential does not explicitly include partial charges. The parameters and functional form of the UFF can be found in previous work [14,15].

We perturbed the UFF potential in two ways. In the first parametric sensitivity analysis, we maintained the UFF prescription that the parameters describing the interactions be the same for each type of atom. Thus, there is only one type of fluorine atom in the original UFF formulation. Therefore, in this first analysis, we strictly varied the magnitude of several key potential parameters, such as the equilibrium bond distance and force constant of the CO and CF bond stretching modes, the equilibrium bond angle and force constant of the COC and CCO bond bending modes, the energy barrier of the OCCO and FCCF bond torsion modes, and the size and energetic well-depth describing all the non-bonded interactions between F, C and O.

We also perturbed the UFF potential in a second way. We allowed the parameters describing the non-bonded interactions of fluorine to vary with the location of fluorine within the molecule. Specifically, we defined different types of fluorine atoms, depending upon their relative proximity to the O in the ether linkage. In figure 2(a),

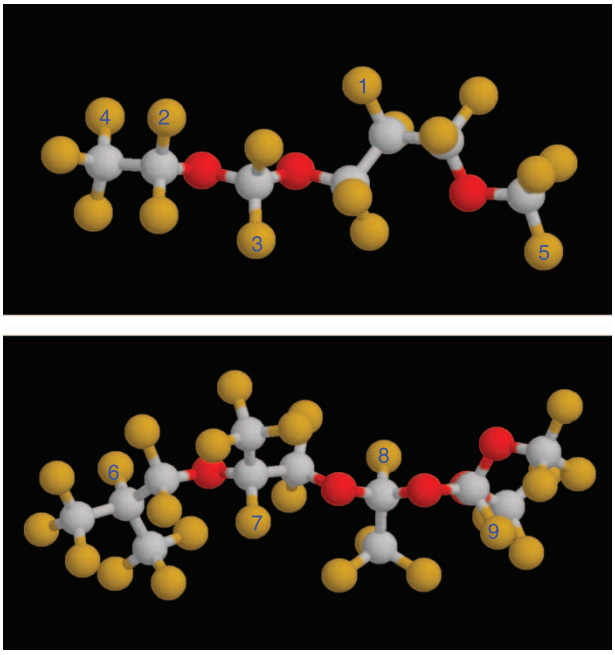

Figure 2. Types of fluorine in PFPEs. The F atom is defined by the atoms to which the adjacent carbon is bound. (a) In a linear PFPE, we have five groups centered on C atoms: (1) CF_2C_2, (2) CF_2CO, (3) CF_2O_2, (4) CF_3C, and (5) CF_3O. (b) In a branched PFPE, we have four additional groups: (6) CFC_3, (7) CFC_2O, (8) $CFCO_2$, and (9) CFO_3.

we provide a schematic of a hypothetical linear PFPE that shows each of these five different types of fluorine atoms. Specifically, the F atom is defined by the atoms to which the adjacent carbon is bound. In the linear PFPE of figure 2(a), we have five groups centered on carbon atoms: (1) CF_2C_2, (2) CF_2CO, (3) CF_2O_2, (4) CF_3C, and (5) CF_3O. This is a complete set of groups for linear PFPEs. For branched PFPEs, four additional groups are possible: (6) CFC_3, (7) CFC_2O, (8) $CFCO_2$, and (9) CFO_3, as shown in figure 2(b). To our knowledge, groups (8) and (9) do not appear in commercial PFPEs and are included solely for completeness. For the four linear PFPEs studied in this work, we have only four types of fluorine atoms, corresponding to numbers (2)–(5) in figure 2(a).

Our motivation in choosing to focus on the fluorine atoms (rather than carbon) is the fact that the highly electronegative fluorine group is larger and more susceptible to behave differently in local environments than carbon. Clearly, the definition of the multiple types of fluorine atoms allows us to reproduce the experimental PFPE rheological properties more closely, if only due to the increase in the number of parameters. Therefore, it was our initial goal to use the single type of fluorine and optimize the parameters. It was only after painstakingly searching through the 50-plus-dimensional parameter space of the UFF potential, through a parameter sensitivity analysis, that we concluded that we could not qualitatively capture the trend in experimental viscosities. Thus, we moved to defining multiple fluorine atom types. It is worth noting that Li *et al.* similarly defined different fluorine atoms in PFPEs when using molecular simulation to predict vapor–liquid equilibria [17–19]. For brevity in the remainder of the document, we refer to these potentials as single fluorine (SF) and multiple fluorine (MF) potentials.

As an aside, in preliminary studies, we also evaluated an explicit atom potential that included partial charges, specifically, the consistent valence force field (CVFF) [13,20], in order to determine whether the inclusion of electrostatic effects via partial charges was essential. Because: (i) CVFF and UFF potentials gave qualitatively similar results for the trend of the viscosity with respect to molecular architecture, and (ii) because of the work of Li *et al.* showing the importance of different types of fluorine atoms, we proceeded by perturbing just the UFF potential.

We acknowledge that the reparameterization that we are performing is solely based on capturing the correct trends in the viscosity with respect to temperature and molecular architecture of the lubricant. This reparameterization will also affect thermodynamic properties such as the equation of state. We do not focus on that element in this work. Rather, we limit ourselves to NEMD simulations in the NVT ensemble where the density is provided from theory or experimental data, which is a common practice for NEMD simulations in which one is interested in the dependence of the viscosity on the molecular architecture of the material and/or the temperature [14,21–26].

2.2 Simulation technique

Both NVT equilibrium molecular dynamics (EMD) and NEMD simulations were performed for all four compounds in figure (1). For both types of simulations, the multiple time-step method known as the reversible reference system propagator algorithm (r-RESPA) [27] was combined with a Nosé–Hoover thermostat [28,29] to integrate the equations of motion. The large time step was 2.0 fs for the intermolecular interactions and thermostat, and the small time step was 0.2 fs for the intramolecular interactions. In the NEMD simulations, we imposed planar Couette flow (PCF), for which the SLLOD [30] algorithm (equivalent to p-SLLOD [31] in shear flows) is appropriate, to generate the trajectories of particles. The Lees–Edwards [32] periodic boundary condition for NEMD PCF simulation was applied.

The simulations contained 216 molecules, corresponding from 4968 to 6480 atoms depending on the PFPE. A cut-off distance of 12.5 Å was used for all the non-bonded interactions. For each compound, an artificially high temperature, 673 K, was used to accelerate the initial configuration to reach equilibrium in the EMD simulations. The equilibrated configurations were attained in 5–10 ns, based on the different compounds studied. Then EMD simulations were carried out at different (lower) temperatures for additional 1–3 ns before determining if the system had attained equilibrium at the new temperature. As for the NEMD simulations, the equilibrated configurations were used as starting points. The duration of the simulations depended strongly on the strain rate and temperature, both of which strongly influence the time it takes to reach steady state [14]. The lower the shear rate, the longer time it takes for the system to reach steady state. Generally, the time required to reach steady state is proportional to the relaxation time of system. Simulation durations ranged from 25 to 75 ns. At the lowest shear rate for all compounds at 253 K, 50 ns of simulation time was necessary to reach steady state. This was carefully checked by monitoring the end-to-end distance, conformation tensor, and the distribution functions of torsion and bending angles. Data were only collected over a period of at least 10 ns after a steady state was attained, with sampling every 10 ps.

2.3 Experimental procedure

The PFPEs used in this study were synthesized by the direct aerosol fluorination process developed by Adcock *et al.* [33–35]. This technique involves the adsorption of organic compounds onto NaF aerosol particles, followed by the free radical addition of elemental fluorine. Unwanted side reactions are minimized by dilution of fluorine with helium and low temperatures (−20°C for the first stage of the reaction, 0°C for the second stage). Perfluorination of the ethers is achieved by a UV photochemical finishing stage. The compounds used in this study were obtained from commercial sources

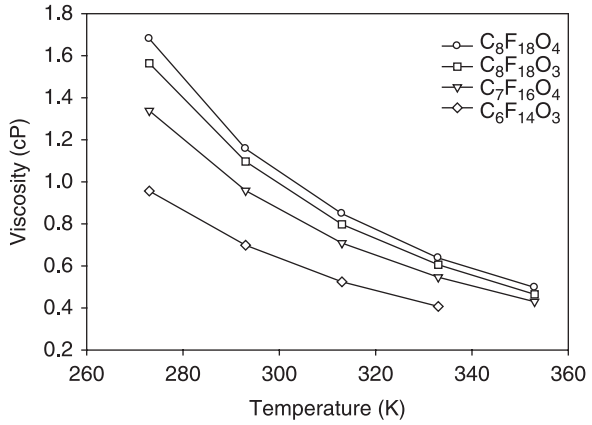

Figure 3. The Newtonian viscosity in the Newtonian plateau region vs. temperature for the four PFPE compounds from experiment.

(Aldrich and Acros Organics) and kept under dry nitrogen until needed. A typical synthesis involves the controlled delivery of the ether at 1 ml/h to the aerosol fluorinator. The crude product from the reactor is isolated through fractionation on a vacuum line, and perfluorination is confirmed by FTIR using a Bomem infrared spectrometer. Purification of each compound is accomplished by using a Bendix 2300 gas chromatograph with a SE-52 column. A center-cut is taken from the major product (purity $\geqq 99\%$), and the structure is confirmed by ^{19}F NMR using a Varian 300 MHz NMR instrument. The viscosity was measured with the Cannon-Manning Semi-Micro Viscometer, manufactured by Cannon Instrument Co.

3. Comparison of results from simulations and experiment

3.1 Shear viscosities from experiment

In figure 3, we plot the experimentally determined shear viscosity for each of the four compounds as a function of temperature. At all temperatures, we observe the same trends in viscosities, namely that $C_8F_{18}O_4 > C_8F_{18}O_3 > C_7F_{16}O_4 > C_6F_{14}O_3$, or *base* > *end* > OCO > *short*. By comparing the *base* and *short* PFPEs, we see that the viscosity decreases with chain length. This is explained by the fact that the shorter chains have smaller rotational relaxation times, which translate into lower viscosities. This is also the case with linear alkanes [23].

By comparing the *short* and *end* PFPEs, we see that the larger CC end groups on the end molecules result in higher viscosities. This can be attributed again strictly to the known dependence of viscosity on chain length. By comparing the *base* and the OCO PFPEs, we see that the presence of the OCO link in the OCO PFPE lowers the viscosity. The argument for this effect stems from the fact that adjacent CF_2 groups cause a ratcheting configuration between the large fluorine atoms, which results in a very stiff chain. A single CF_2 group surrounded by oxygen atoms provides additional flexibility to the chain, which lowers the rotational relaxation time and the viscosity. One might argue that the OCO PFPE (backbone of 11 atoms) is also shorter than the *base* PFPE (backbone of 12 atoms) and that this effect might strictly be explained in terms of chain length rather than the increased flexibility of the

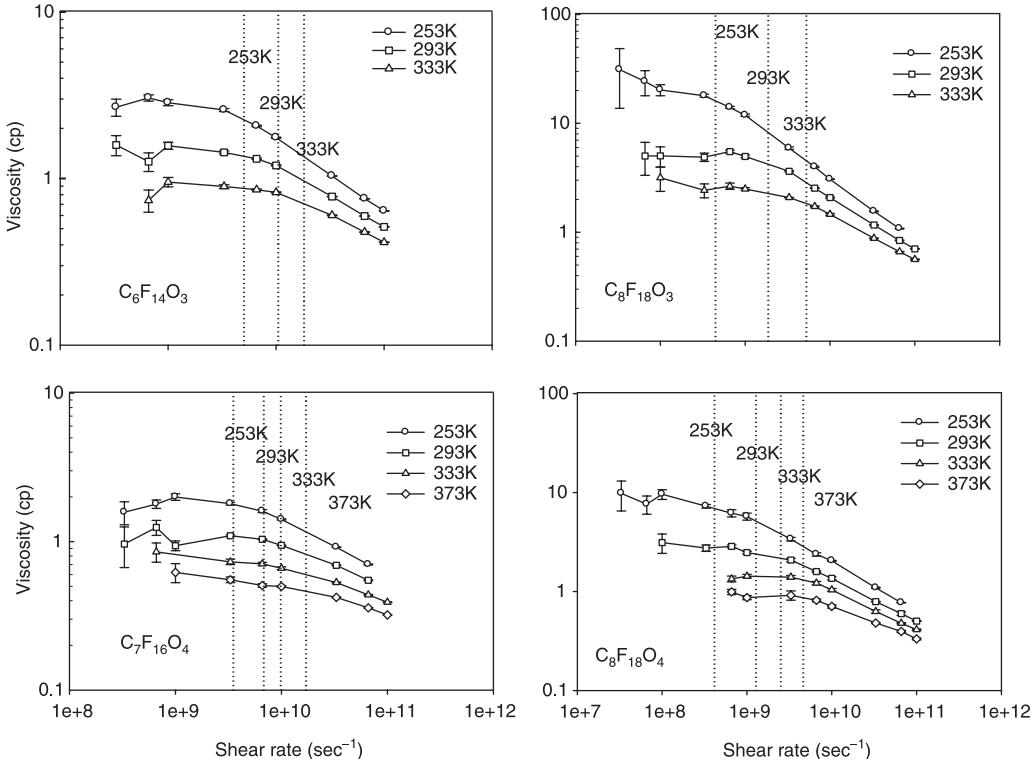

Figure 4. The shear viscosity vs. shear rate at different temperatures for compounds $C_6F_{14}O_3$, $C_7F_{16}O_4$, $C_8F_{18}O_3$ and $C_8F_{18}O_4$ using the SF potential.

OCO group. However, by comparison of the OCO PFPE and the *end* PFPE, both of which have the same number of atoms in the backbone, we do indeed observe that the OCO PFPE has a lower viscosity, reinforcing the belief that the OCO group provides additional chain flexibility.

3.2 Shear viscosities from NEMD simulations with the single fluorine potential

Shear viscosities from NEMD simulations using the SF potential with the published UFF parameters at different shear rates and temperatures for $C_6F_{14}O_3$, $C_7F_{16}O_4$, $C_8F_{18}O_3$ and $C_8F_{18}O_4$ are shown in figure 4. The vertical dotted lines represent the critical shear rates (the inverse of rotational relaxation times). The relaxation times were calculated through fitting the time autocorrelation function of the end-to-end distance in EMD simulations [14,36]. The four compounds exhibit qualitatively similar behavior under shear flow. The Newtonian plateau appears at low shear rates. We should note that the lowest shear rate in this simulation is at a magnitude of 10^7, and the lowest critical shear rate is at a magnitude of 10^8, which is beyond the range of a typical viscometer, but is sufficient to explore a portion of the Newtonian plateau. After the Newtonian plateau, we observe shear-thinning of the viscosity for each compound. Figure 4 also shows that the critical shear rates for each compound increase (the relaxation times decrease) and the shear viscosities decrease with the increasing temperatures. The difference in shear viscosity between temperatures for each compound is clearly significant at low shear rate, but decreases with increasing shear rate.

In figure 5, the viscosities in the Newtonian plateau region from simulation and experiment are plotted as functions of temperature. If we compare the magnitude of the Newtonian viscosity of the four compounds from NEMD at the same temperature and shear rate, the order is $C_8F_{18}O_3 > C_8F_{18}O_4 > C_6F_{14}O_3 > C_7F_{16}O_4$, or end > base > short > OCO. Not only are the magnitudes of the viscosity too high relative to experiment by factors ranging from 2 to 10, but, more importantly, the relative trend among compounds is incorrectly predicted. This renders the SF potential with UFF parameters totally unsuitable for the purposes of examining the relationship between lubricant molecular architecture and rheological properties.

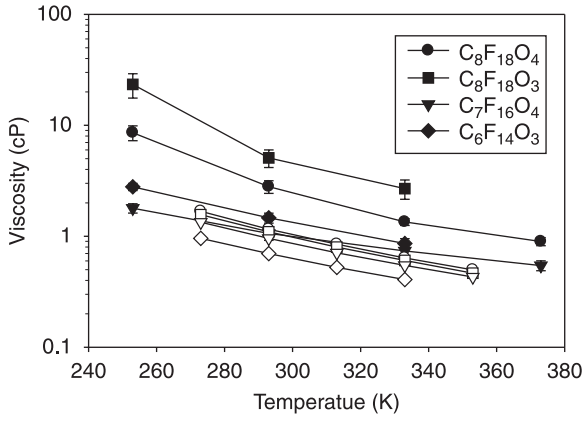

Figure 5. The Newtonian viscosity vs. temperature for the four compounds using the SF potential. The filled symbols represent results from NEMD simulations using the original UFF force field, and the hollow symbols represent the results from experiment.

The quantitative mismatch between experiment and simulation is not a serious concern since it is possible to find parameters that can alter the magnitude of the simulated viscosities. The failure of the SF potential with UFF parameters to capture the trend is much more serious and is explained by the over-prediction of the chain flexibility resulting from the ether linkage. For example, an incorrect trend is predicted from simulation for the *base* and *end* PFPEs. In experiment, the longer (more atoms in the backbone) *base* PFPE has a higher viscosity, whereas in simulation, the *end* PFPE with only three O atoms in the backbone (compared to four O atoms in the *base* PFPE) has a higher viscosity. Similarly, we have the incorrect trend with respect to the OCO and *short* PFPEs. In experiment, the longer OCO PFPE has a higher viscosity, whereas in simulation, the *short* PFPE with only three O atoms in the backbone (compared to four O atoms in the OCO PFPE) has a higher viscosity.

With such direct evidence for the cause of discrepancy between simulation and experiment, it is necessary to modify selected potential parameters which control the relative F and O contributions to the flexibility of the chain. To this end, we explored changing the parameter value while maintaining the SF potential.

Since the original UFF force field overestimates the viscosity (meaning the rotational relaxation time is too long, which in turn means that the chain is too stiff), it is natural to check the size of fluorine atom by changing Lennard–Jones collision diameter, σ_F. The effect σ_F on viscosities of compounds $C_8F_{18}O_4$ (*base*) and $C_8F_{18}O_3$ (*end*) at 293 K is shown in figure 6. Recall that experimentally, the viscosity of the *base* PFPE is greater than that of the *end* PFPE. Figure 6 shows that σ_F has a strong effect on the viscosity of the PFPEs. The viscosity generally decreases with decreasing fluorine size. For this reason, modifying the magnitude of the viscosity for a single compound by a factor of ten can be achieved by very modest changes in several key parameters. However, figure 6 clearly illustrates that changing σ_F does not result in the reversal of the relative values of the *base* and *end* PFPEs. Therefore, we conclude that the size of the fluorine atom is not the main source of inconsistency between experiment and simulation.

In an attempt to enhance chain flexibility, one can also examine the dihedral bond torsion potential connecting atoms 1–2–3–4. It is important to realize in the UFF potential that non-bonded interactions are included between the 1 and 4 atoms, and that the parameters of the torsion potential itself are only functions of atoms 2 and 3. Therefore, the net torsion potential is a combination of the explicit torsion potential and the non-bonded 1–4

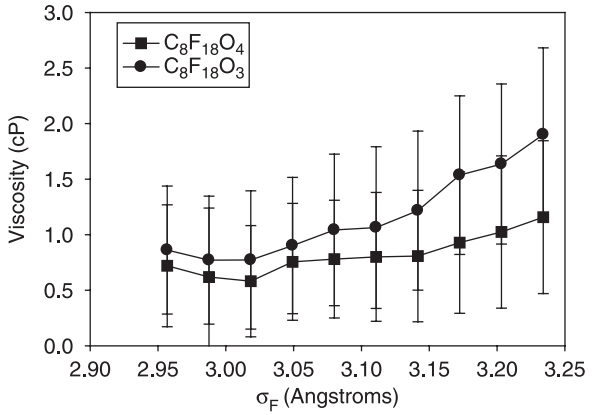

Figure 6. Effect of the Lennard–Jones distance σ_F on the viscosities of compounds: $C_8F_{18}O_4$ (*base*) and $C_8F_{18}O_3$ (*end*) at 293 K (the shear rate is $3.3 \times 10^9\ s^{-1}$).

interaction. When the 1–4 atoms are very large, like F, the repulsive interaction between fluorine atoms dominates. Therefore, the changes shown in figure 6 also reflect a change in the net torsional interaction.

We also performed dozens of other trials within the SF potential, exploring changes in parameters singly and in combination. For example, we also examined weakening the interaction between fluorine in the CF_2CF_2 groups, varying the parameters of bond stretching and bending, by changing the well depths of atoms in non-bonded interactions. While many of these parameter changes had drastic effects on the magnitude of the viscosity, none of these parameter changes could correct the relative trend in the viscosity among compounds. At this point, we began to explore the MF potential.

3.3 Shear viscosities from NEMD simulations with the multiple fluorine potential

Reports in the literature [17–19] suggest that the size of a fluorine atom changes in response to its environment, which means that the Lennard–Jones collision diameter of fluorine, σ_F, should be altered accordingly (figure 2). Re-parameterization of the four types of fluorine atoms, which constitute the sample compounds, is based on the viscosities as determined experimentally at 293 K. The adjusted parameters for the MF potential are listed in table 1. It is worth noting that the functional form of the potential is unaltered from the UFF prescription. The sole difference lies in the choice of the parameters for the non-bonded interactions involving fluorine.

Table 1. Parameters of the non-bonded interaction for different types of fluorine atoms in the MF potential.

Fluorine type	*CF_3O*	*CF_2CO*	*CF_3C*	*CF_2O_2*	*F**
ε/k_B (K)	25.16	25.16	25.16	21.39	25.16
σ (Å)	3.224	3.100	3.100	3.193	3.36

F* represents the fluorine atom in the original UFF.

This re-parameterization of the MF potential allowed the correct experimental trends to be reproduced by simulation. Insight is obtained by examining the various types of fluorine atoms in each of the four compounds. The *base* PFPE has 6 fluorines of type 5, and 12 fluorines of type 2; the *short* PFPE has 6 fluorines of type 5, and 8 fluorines of type 2; the *end* PFPE has 6 fluorines of type 4, and 12 fluorines of type 2; and the OCO PFPE has 6 fluorines of type 5, 8 fluorines of type 2, and 2 fluorines of type 3. Since the *end* PFPE is the only compound that has fluorine of type 4, there exists an independent tuning parameter to adjust its viscosity. Similarly, since the OCO PFPE is the only compound that has fluorine of type 3, there is another independent tuning parameter to adjust its viscosity. As mentioned above, the adjustment of the magnitude of the viscosity of a single compound is straightforward.

The results from the optimized MF potential are compared with experimental data at 293 and 333 K in figure 7. The viscosities from simulation were obtained through averaging the values in the Newtonian plateau regions. Figure 7 shows that the viscosities calculated from the MF potential are well matched with experimental data. Moreover, the values of the viscosities from simulation are consistent with the experimental data at both temperatures. The average error between simulation and experiment is 5%. The MF potential corrected both the relative trends and absolute values of the viscosities.

In figure 7, we fit the parameters to the data at 293 K and predicted the data at 333 K. At 333 K, we maintained the accuracy of the fit to the experimental data at 293 K, illustrating that the chosen parameters captured the temperature dependence of the viscosity. It is also important to examine how the changes in the size of the fluorines affect other properties.

The temperature dependency of rotational relaxation times is shown in figure 8. In both the original SF and MF UFF force field cases, the relaxation time decreases with increasing temperature. The order of the relaxation times is consistent with the sequence of molecular length of the

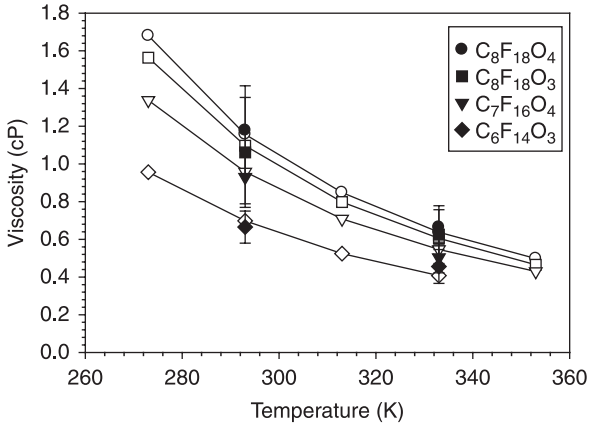

Figure 7. The shear viscosity vs. temperature for the four compounds. The filled symbols represent results from NEMD simulations using the MF potential, and the unfilled represent the results from experiment.

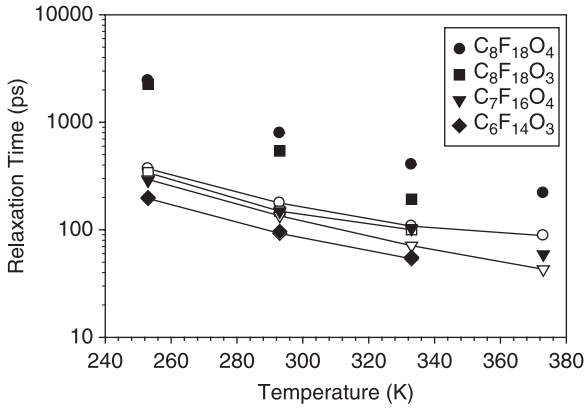

Figure 8. Temperature dependence of the relaxation times obtained through the SF and MF potentials. Filled and unfilled symbols represent the results of the SF and MF potentials, respectively. Note that filled and unfilled diamonds overlap.

four compounds examined. The difference between relaxation times of the SF and MF potentials for $C_8F_{18}O_4$ (*base*) and $C_8F_{18}O_3$ (*end*) is fairly significant, which is the primary reason for the alteration of viscosities between the two potentials: generally, the viscosity of short-chains in the Newtonian plateau region is proportional to the relaxation time, according to the Upper-Convected Maxwell Model of polymer rheology [21]. For $C_6F_{14}O_3$ (*short*) and $C_7F_{16}O_4$ (OCO), the relaxation times obtained using the MF potential also decrease slightly from the original SF potential.

Figure 9 displays the shear rate dependence of the mean-squared end-to-end distance ($\langle R^2_{ete}\rangle$) of chains at 293 K, as obtained using the original SF and MF potentials. Overall, $\langle R^2_{ete}\rangle$ does not change significantly with respect to shear rate, although minor decreases can be observed at high shear rates. The fact that these PFPEs do not extend significantly in the presence of shear (in contrast to linear alkanes) is due to the presence of the fluorine atoms, which stiffen the chains. The order of $\langle R^2_{ete}\rangle$ is strictly consistent with the length of the molecular chain. However, the alteration of $\langle R^2_{ete}\rangle$ when replacing the

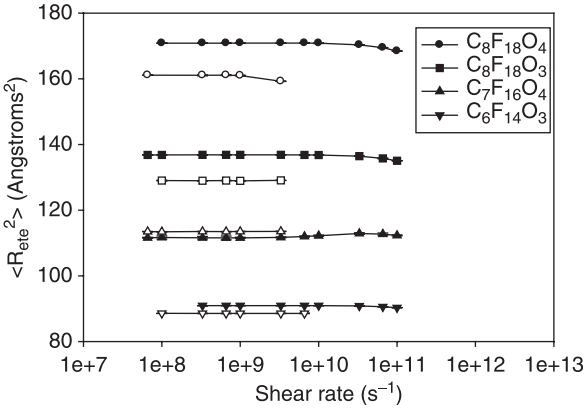

Figure 9. Shear rate dependence of the mean-squared end-to-end distance ($\langle R^2_{ete}\rangle$) of chains at 293 K obtained using the SF and MF potentials. Filled and unfilled symbols represent the SF and MF potentials, respectively.

SF potential with the MF potential is different among the four compounds. For $C_8F_{18}O_4$, $C_8F_{18}O_3$ and $C_6F_{14}O_3$, $\langle R^2_{ete}\rangle$ decreases when changing from the SF to the MF potential, but for $C_7F_{16}O_4$ (OCO), $\langle R^2_{ete}\rangle$ increases. The different performances are explained by the way the non-bonded interaction parameters were revised. The OCO PFPE is too flexible in the SF potential. In the MF potential, the comparatively larger size of fluorine in the CF_2O_2 group primarily contributes to the increase of $\langle R^2_{ete}\rangle$, since the changes of the other types of fluorine atoms in $C_7F_{16}O_4$ decrease $\langle R^2_{ete}\rangle$.

4. Conclusions

We have reported shear viscosities for four PFPE compounds from non-equilibrium molecular dynamics simulation and from experiment. We determined that an explicit-atom potential that treats all fluorine atoms equivalently was not capable of reproducing the experimentally observed trends in viscosity among the four compounds. Rather, we found that the parameters of the potential governing the interactions of fluorine atoms must reflect the proximity of the fluorine to the oxygen in the ether linkage. Defining four different types of fluorine atoms, we were able to reproduce the experimentally observed trends in viscosity of the four compounds. These changes in parameters affect the stiffness of the chains, which manifest as changes in the average end-to-end distance of the chain. This in turn alters the rotational relaxation times of the compounds, which ultimately controls their viscosities.

Acknowledgements

This work has been supported by Air Force Office of Scientific Research through contract # FA 9550-05-1-0342. The authors wish to acknowledge resources of the Center for Computational Sciences at Oak Ridge National Laboratory, which is supported by the Office of Science of the DOE under Contract DE-AC05-00OR22725.

References

[1] G.A. Bell, J. Howell, T.W.D. Pesco. Perfluoroalkylpolyethers. In *Synthetic Lubricants and High-Performance Functional Fluids*, L.R. Rudnick, R.L. Shubkin (Eds.), p. 215, Marcel Dekker, Inc., New York (1999).

[2] L.S. Helmick, L.J. Gschwender, S.K. Sharma, C.E. Snyder Jr., J.C. Liang. The effect of humidity on the wear behavior of bearing steels with $R_fO(n\text{-}C_3F_6O)_xR_f$ perfluoropollyalkylether fluids and formulations. *Trib. Trans.*, **40**(3), 393 (1997).

[3] M.S. Jhon. Physicochemical properties of nanostructrured perfluoropolyether films. In *Advances In Chemical Physics*, S.A. Rice (Ed.), Vol. 129, p. 1, John Wiley & Sons, Inc., New York (2004).

[4] C.E. Snyder Jr., L.J. Gschwender, O.L. Scott. Characterization of model perfluoropolyalkylethers by miniaturized thermal oxidative thechniques—part II: pressure differential scanning calorimetry. *Trib. Trans.*, **38**(3), 733 (1995).

[5] L.J. Gschwender, S.K. Sharma, C.E. Snyder Jr, F.G.W.S. Bruce. The effect of additives on the wear behavior of bearing steels with $R_fO(CF_2O)_xCF_2CF_2O)y(CF_2CF_2CF_2O)_zR_f$ perfluoropolyalkylether fluids. *Trib. Trans.*, **41**(1), 78 (1998).

[6] Y. Tanaka, N. Nojiri, K. Ohta, H. Kubota, T. Makita. Density and viscosity of linear perfluoropolyethers under high-pressures. *Int. J. Thermophys.*, **10**(4), 857 (1989).

[7] R.N. Kono, I.S.M.S. Jhon, C.A. KIm, H.J. Choi. Rheology of perfluoropolyether lubricant. *IEEE Trans. Magn.*, **37**(4), 1827 (2001).

[8] Q. Guo, P.S. Chung, H. Chen, M.S. Jhon. Molecular rheology of perfluoropolyether lubricant via nonequilibrium molecular dynamics simulation. *J. Appl. Phys.*, **99**, 08N105 (2006).

[9] Q. Guo, S. Izumisawa, D.M. Phillips, M.S. Jhon. Surface morphology and molecular conformation for ultrathin lubricant films with functional end groups. *J. Appl. Phys.*, **93**(10), 8707 (2003).

[10] Q. Guo, S. Izumisawa, M.S. Jhon, Y.-T. Hsia. Transport properties of nanoscale lubricant films. *IEEE Trans. Magn.*, **40**(4), 3177 (2004).

[11] X. Li, Y.-Z. Hu, H. Wang. A molecular dynamics study of lubricant perfluoropolyther in hard disk driver. *Acta Phys. Sin.*, **54**(8), 3787 (2005).

[12] A. Koike. Molecular dynamics study of tribological behavior of confined branched and linear perfluoropolyethers. *J. Phys. Chem. B*, **103**, 4578 (1999).

[13] D. Kamei, H. Zhou, K. Suzuki, K. Konno, S. Takami, M. Kubo, A. miyamoto. Computational chemistry study on the dynamics of lubricant molecules under shear conditions. *Tribol. Int.*, **36**, 297 (2003).

[14] B. Jiang, D.J. Keffer, B.J. Edwards. Estimation and analysis of the rheological properties of a perfluoropolyether through molecular dynamics simulation. *J. Fluor. Chem.*, **127**, 787 (2006).

[15] A.K. Rappe, C.J. Casevit, K.S. Colwell, W.A. Goddard, W.M. Skiff. UFF, a full periodic table force field for molecular mechanics and molecular dynamics simulations. *J. Am. Chem. Soc.*, **114**, 10024 (1992).

[16] C. MCCabe, D. Bedrov, O. Borodin, G.D. Smith, P.T. Cummings. Transport properties of perfluoroalkane using molecular dynamics simulation: comparison of united- and explicit-atom models. *Ind. Eng. Chem. Res.*, 42 (2003).

[17] H.-C. Li, C. McCabe, S.T. Cui, P.T. Cummings, H.D. Cochran. Development of a force field for molecular simulation of the phase equilibria of perfluoro-methyl-propyl ether. *Mol. Phys.*, **100**, 265 (2002).

[18] H.-C. Li. Molecular modeling of perfluoro compounds. Phd dissertation, University of Tennessee (2001)

[19] H.-C. Li, C. McCabe, S.T. Cui, P.T. Cummings, H.D. Cochran. On the development of a general force field for the molecular simulation of perfuoropolyethers. *Mol. Phys.*, **101**, 2157 (2003).

[20] P. Dauber-Osguthorpe, V.A. Roberts, D.J. Osguthorpe, J. Wolff, M. Genest, A.T. Hagler. Structure and energetics of ligand binding to proteins: *Escherichia coli* dihydrofolate reductase-trimethoprim, a drug-receptor system. *Protein Struct. Funct. Genet.*, **4**(1), 31 (1988).

[21] C. Baig, B. Jiang, B.J. Edwards, D.J. Keffer, H.D. Cochran. A comparison of simple rheological models and simulation data of n-hexadecane under shear and elongational flows. *J. Rheo.*, **50**(5), 625 (2005).

[22] C. Baig, B.J. Edwards, D.J. Keffer, H.D. Cochran, H. VA. Rheological and structural studies of linear polyethylene melts under planar elongational flow using nonequilibrium molecular dynamics simulations. *J. Chem. Phys.*, **124**(8), 084902 (2006).

[23] C. Baig, B.J. Edwards, D.J. Keffer, H.D. Cochran. Rheological and structural studies of liquid decane, hexadecane, and tetrasosane under planar elongational flow using nonequilibrium molecular dynamics simulations. *J. Chem. Phys.*, **122**(1), 184906 (2005).

[24] S.T. Cui, P.T. Cummings, H.D. Cochran. Multiple time step nonequilibrium molecular dynamics simulation of the rheological properties of liquid n-decane. *J. Chem. Phys.*, **104**(1), 255 (1996).

[25] S.T. Cui, S.A. Gupta, P.T. Cummings. Molecular dynamics simulations of the rheology of normal decane, hexadecane, and tetracosane. *J. Chem. Phys.*, **105**(3), 1214 (1996).

[26] P.J. Daivis, D.J. Evans. Comparison of constant pressure and constant volume nonequilibrium simulations of sheared model decane. *J. Chem. Phys.*, **100**, 541 (1994).

[27] M. Tuckerman, B.J. Berne, G.J. Martyna. Reversible multiple time scale molecular dynamics. *J. Chem. Phys.*, **97**(3), 1990 (1992).

[28] W.G. Hoover. Canonical dynamics: equilibrium phase-space distributions. *Phys. Rev. A*, **31**, 1695 (1985).

[29] S. Nosé. A unified formulation of the constant temperature molecular dynamics methods. *J. Chem. Phys.*, **81**, 511 (1984).

[30] D.J. Evans, G.P. Morris. *Statistical Mechanics of Nonequilibrium Liquids*, Academic, New York (1990).

[31] C. Baig, B.J. Edwards, D.J. Keffer, H.D. Cochran. A proper approach for nonequilibrium molecular dynamics simulations of planar elongational flow. *J. Chem. Phys.*, **122**, 114103 (2005).

[32] A.W. Lees, S.F. Edwards. Computer study of transport processes under extreme conditions. *J. Phys. Part C Solid*, **5**, 1921 (1972).

[33] J.L. Adcock, M.L. Cherry. Aerosol direct fluorination: direct synthesis of perfluorinated glyme ethers. *J. Fluor. Chem.*, **30**, 343 (1985).

[34] J.L. Adcock, K. Horita, E.B. Renk. Low-temperature fluorination of aerosol suspensions of hydrocarbons utilizing elemental fluorine. *J. Am. Chem. Soc.*, **103**, 6937 (1981).

[35] J.L. Adcock, M.L. Cherry. Aerosol direct fluorination: a developing synthesis technology and an entry level mechanistic tool. A short review. *Ind. Eng. Chem. Res.*, **26**(2), 208 (1987).

[36] J.M. Haile. *Molecular Dynamics Simulation: Elementary Methods*, Johon Wiley & Sons, Inc., New York (1992).